

# DETERMINATION OF ORBITAL AND SPIN PARAMETERS OF LEO SATELLITES BY POLISH AND UKRAINIAN OPTICAL OBSERVATORIES

K. Kamiński<sup>(1)</sup>, N. Koshkin<sup>(2)</sup>, L. Shakun<sup>(2)</sup>, J. Golebiewska<sup>(1)</sup>, E. Korobeinikova<sup>(2)</sup>, and E. Wnuk<sup>(1)</sup>

<sup>(1)</sup>*Astronomical Observatory Institute, Faculty of Physics, A.Mickiewicz University, Stoleczna 36, 60-286 Poznań, Poland, Email: chrisk@amu.edu.pl*

<sup>(2)</sup>*Astronomical Observatory of Odessa I.I.Mechnikov University, #1B, Marazlievskaya St., Odessa, 65014, Ukraine, Email: nikkoshkin@yahoo.com*

## ABSTRACT

A joint Polish-Ukrainian astrometric and photometric observing campaign has been performed in January and February of 2017. Several LEO objects were observed using satellite tracking optical sensors from the Astronomical Observatory of Odessa University and the Astronomical Observatory of Adam Mickiewicz University in Poznań. Data series obtained using two different observing, reduction and analysis techniques have been successfully analysed. Orbital fitting of data from two sensors located on different continents shows consistency at the level of a few arcseconds. The best strategy for future improvements, that should enable the reduction of individual position errors even below 1 arcsec, has been identified.

Additionally, a method to estimate the spin parameters of big space debris using fast photometry is presented. There is a collection of 7.5 thousand photometric curves for over 500 objects obtained in the years 2005-2016 in Odessa Observatory. For several inactive satellites the variations of sidereal spin periods and spin axis directions have been determined. In this paper the joint photometric data and the rotation of the big inactive satellites Envisat and Topex/Poseidon were analyzed. The deceleration of Envisat's rotation during 4 years was studied together with the estimation of its spin axis inclination.

Keywords: optical observations, orbit determination, spin determination, SST.

## 1. INTRODUCTION

European activities in Space Situational Awareness (SSA) Programme are coordinated by European Space Agency (ESA) and European Commission (EC). ESA SSA Programme is active in three main segments: Space Weather (SWE), Near-Earth Objects (NEO) and Space Surveillance and Tracking (SST). Based on the decision No 541/2014/EU of the European Parliament and the

Council of 16 April 2014 establishing a Framework for Space Surveillance and Tracking Support, five countries: Germany, France, Spain, Italy and the United Kingdom established the SST Consortium in 2015. Several other countries, including Poland, are planning to join the EC SST Consortium. The future SST services provided both by ESA SST System and EC SST Consortium need to monitor satellite and space debris objects orbiting the Earth. All hazardous objects that may potentially cause catastrophic collisions have to be detected, tracked and catalogued. The lower threshold for those objects is at a level of a few centimeters (with 1 cm target). The estimated number of Earth orbiting objects with sizes greater than 1 cm is at least 600 000. A network of effective sensors capable to track such a large number of objects with appropriate accuracy is of the highest importance for the SST system. LEO objects are tracked mainly with the use of radar sensors, while optical telescopes are used to monitor the orbital motion of MEO and GEO objects. However, due to significant progress in the telescope development technology, some contemporary telescopes are able to detect and track very fast moving LEO objects, with a great success, at a high accuracy level. Moreover, optical sensors are significantly cheaper than radar sensors. An appropriate number of optical sensors distributed in optimal geographical locations are able to provide observations of a large number of LEO objects sufficient to maintain the satellite orbit catalog at an accuracy level comparable to that based on radar measurements of LEO objects.

In accordance with the rules established for ESA SST System and EC SST Consortium, each participating country is allowed to declare a list of sensors to be included in the European SST network. It is therefore essential to perform an adequate qualification analysis of each sensor observing capabilities and the quality of its measurements. It is also important to perform an analysis of collaboration possibilities between sensors from different countries.

In this work we present a joint SST campaign of Poznań and Odessa astronomical observatories conducted in 2017. Optical sensors located in Poland (Poznań Observatory), Arizona (Winer Observatory) and Ukraine (Odessa Ob-



Figure 1. KT-50 50 cm telescope of Odessa Observatory.

servatory) have been used for astrometric and photometric observations of selected, bright LEO targets. Different equipment, observing and analysis approaches are compared using ILRS ephemeris as well as separate and combined orbital fits. Rotation speed and axis orientation is also analyzed with fast photometry from Odessa and Arizona.

## 2. EQUIPMENT DESCRIPTION IN ODESSA OBSERVATORY

Satellite observations in Odessa Observatory were obtained using KT-50 located in Odessa ( $46^{\circ}28'40.0''$  N,  $30^{\circ}45'20.3''$  E, 56m). It is a 50 cm cinema theodolite with focal length of 200 cm (Figure 1). The telescope is equipped with the analog video camera WAT-209H2. The field of view of the telescope is  $11' \times 8'$  and the image scale is 0.9 arcsec per pixel. The video camera makes video stream with 25 frames per second. Each frame has two interlaced half frames. The exposure time of the half frame is 0.02sec. All half frames are exposed one by one without discontinuity between them. The video camera sends analog video signal to the TV tuner on a personal computer. Time marks with the number of previous seconds from the GPS receiver are inserted into the video stream (Figure 2). After the acquisition of the image by TV tuner, time marks on the image are identified and transmission time of the image determined. The details of the measurement method of image acquisition time are discussed in the article [3]. This method assures that random errors of the time of image acquisition are at the level of 0.0001 sec and systematic errors are less than 0.01 sec.

## 3. EQUIPMENT DESCRIPTION IN POZNAŃ OBSERVATORY

Satellite observations in Poznań Observatory were obtained using the Global Astrophysical Telescope Sys-

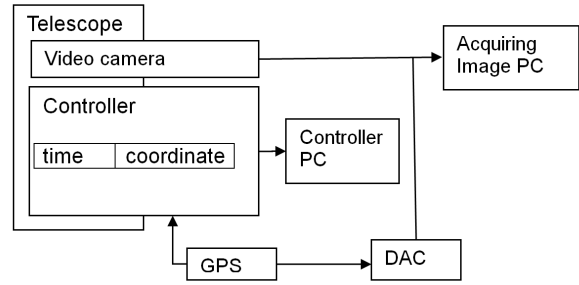


Figure 2. KT-50 telescope control and timing scheme.



Figure 3. PST1 dual 50 cm telescope of Poznań Observatory located in Borowiec in Poland.

tem (GATS) network of optical astronomical telescopes<sup>1</sup>. The network is composed of two instruments: Poznań Spectroscopic Telescope 1 (PST1) established in 2007 and Poznań Spectroscopic Telescope 2 (PST2) established in 2013. The first instrument is located in Borowiec Observing Station in Poland ( $52^{\circ}16'37.2''$  N,  $17^{\circ}04'28.5''$  E, 123.4m) and the second one is located in Winer Observatory in Arizona, USA ( $31^{\circ}39'56.08''$  N,  $110^{\circ}36'06.42''$  W, 1515.7m). While originally not designed specifically for SST observations, both instruments have been upgraded and currently both sensors are able to perform astrometric and photometric measurements of space debris. PST1 is capable to observe targets on MEO, GEO and HEO orbits in sidereal tracking mode, while PST2 can track all satellites, including LEO targets, with non-sidereal velocities up to  $15^{\circ}/s$ .

PST1 is a fully remotely controlled instrument constructed by retrofitting an SBG camera mount with a

<sup>1</sup>[www.astro.amu.edu.pl/GATS](http://www.astro.amu.edu.pl/GATS)

modern computer controlled motors and high resolution optical encoders (Figure 3). On top of this mount two 0.5m newtonian telescopes have been installed and one of them is used for satellite imaging with an SBIG STX-16803 camera. The telescope's field of view is  $1^\circ \times 1^\circ$ , the image scale is 0.92 arcsec per pixel and the camera frame rate (with 2x2 binning) is at the level of 1 image per 6 seconds.

PST2 is a fully robotic Planewave CDK700 telescope. It has an azimuthal direct-drive mount and 70 cm corrected Dall-Kirkham telescope with the focal length of 454 cm. The mount can track with user selectable non-sidereal velocities in both axes, but cannot change those velocities during tracking. One of PST2's Nasmyth foci is used for imaging with an Andor iXon3 888 EMCCD camera. It delivers  $10' \times 10'$  field of view, very high sensitivity when working in electron-multiplying (EM) mode and frame rates up to 6 frames per second (binning 2x2). The exposure time used in this campaign was initially 0.05 sec but later changed to 0.01 seconds due to overexposure of satellite images.

PST1 and PST2 utilize totally different approaches for precise image timing. The PST1's SBIG camera features a relatively slow, mechanical curtain shutter. The time between beginning and end of the shutter movement during shutter opening or closing is about 150ms. As a result, the exposure time is equal on the entire CCD frame, but the beginning and end times vary up to 150ms. It is therefore desirable with this camera to put the target always at the same location on the chip and to use only nearby reference stars. The camera features a trigger-out port providing rectangular signal of shutter opening and closing that can be measured with high accuracy. We constructed a GPS-based event timer that registers every camera's trigger-out signal with an estimated accuracy of at least 0.1 ms. This approach is limited by mechanical delays and irregularities of the movement of camera's shutter, but we estimated the overall precision of the timing system at the level of 30 ms. A dedicated external shutter is considered to be the easiest solution to further increase image timing accuracy.

The PST2's Andor iXon3 EMCCD camera features a global electronic shutter. In contrast to a mechanical shutter or a rolling electronic shutter, it delivers equal exposure start and stop time on every pixel. The camera's SDK contains a low-latency triggering routine that should reduce any delays between executing the software command on a PC and actually starting the exposure on the camera. Our measurements show that some delays are still present and the overall accuracy of this approach is estimated at the level of 10 ms. This might partly be a result of a relatively slow Intel Atom based industrial computer used to control the camera. It is worth noting that newer Andor iXon cameras deliver timing accuracy at the level of 10 ns, according to specification.

The PST2 telescope is a robotic sensor, controlled by a custom designed software capable of orchestrating imaging and spectroscopic observations even though different

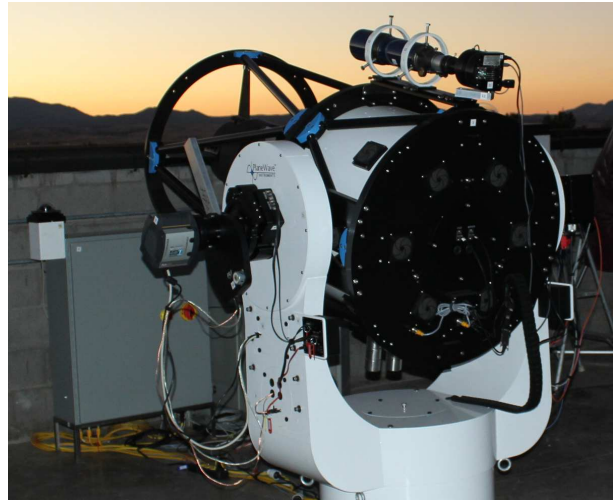


Figure 4. PST2 70 cm telescope of Poznań Observatory located in Winer Observatory in Arizona, USA.

computers are assigned for different pieces of the equipment (Figure 4). The software allows to program a whole night of space debris observations in advance and constantly delivers up to date status through a web-based interface. Two observing modes have been implemented: sidereal tracking and satellite tracking. In sidereal tracking mode the telescope points at given coordinates a few seconds before the satellite passes through and starts a series of frames at the maximum frame rate. The camera is fast and sensitive enough that it is possible to observe even small ( $\sim 20$  cm) LEO targets in this mode. In satellite tracking mode the telescope also points at the given location in advance, but then starts tracking at a selected, constant RA and Dec rate. This mode boosts the sensitivity of the telescope even further, allowing us to observe even the smallest objects in TLE catalogue. Both modes can be repeated many times during the satellite's passage over the observatory in a so-called "leap frog" observing strategy.

An automatic scheduler has also been developed that automatically prepares an observing plan for a given telescope. It takes into account various selection criteria, such as the telescope mount speed and acceleration, meridian and altitude limits, tracking speed limits, stellar field density, bright stars proximity, etc. Also, individual satellite requirements are taken into account, such as target priority, length of image series and number of observations required per satellite passage. Using the scheduler, a list of commands applicable directly into the telescope control software is prepared. Satellite ephemeris are based on the USSTRATCOM TLE catalog and SGP/SDP algorithms. Its accuracy is sufficient for PST1 with  $1^\circ \times 1^\circ$  FoV, but is not always enough for PST2 with its small  $10' \times 10'$  FoV. We estimate that the errors and inaccuracies in the TLE catalog and SGP models account for about 30% of the situations when PST2 misses its target. The other 70% are caused mainly by delays in the telescope's firmware when executing a non-sidereal tracking command. In the sidereal tracking mode about

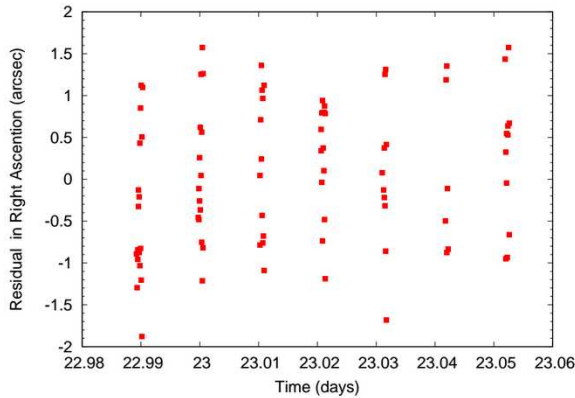


Figure 5. PST1 telescope astrometric measurements of a Galileo satellite. Standard deviation in RA with respect to a fitted model is 0.8 arcsec while in Dec is 0.5 arcsec.

95% of targets are detectable in the telescope's FoV.

Our analysis of satellite astrometry obtained using PST1 telescope shows (Figure 5) that its internal astrometric consistency when observing a MEO satellite is at the level of 0.8 arcsec. This uncertainty is dominated by random errors in measuring times of opening and closing the camera's shutter. Extrapolating these results to several tens times faster moving LEO targets, we estimated the sensor's accuracy at the level of 10-20 arcsec. Considering this limitation and the fact that the telescope is currently unable to track LEO targets, we decided that we will exclude this sensor from the observing campaign, which involved only LEO satellites.

#### 4. DATA REDUCTION AND ASTROMETRY IN ODESSA

After image acquisition, the time mark is decoded and removed, master dark frame is subtracted and the image is rescaled with the flat field. After that, each interlaced frame is splitted in two parts, containing only every second row of the full frame and each half-frame is processed separately. In every half-frame the missing rows are complemented by a copy of the existing rows. Low frequency filtering based on information from the coordinate sensors is used for objects detection. For ultrafaint objects several consecutive frames are combined, taking into account residual shifts of the telescope. For measuring the object pixel coordinates two methods are used: averaging of the object pixel coordinates weighted by brightness of the pixels, or fitting of the prior point spread function (psf) to the object's image. With image exposure of much less than two seconds the atmospheric distortions are not averaged. Hence, the a priori point spread function is not a very good approximation of the visible object's image. Both methods have been used previously (see for example [3]) and similar results have been obtained for non-elongated objects. With elongated

objects a psf similar to the psf used in the work [2] is used.

In the majority of cases only one star in a frame is visible. In such a case it is impossible to determine the full transformation between the image and the celestial coordinate systems. Therefore, average transformation determined before is used and only the zero point of the coordinate frame is corrected for each image. In the rare case when the number of stars in the frame is greater than 3 we attempt to refine the average angle of rotation for current transformation. The final error of the observations includes the random error of the measurement of the object's position in the image and the error caused by differences between the average and true transformation. The main source of transformation error is the telescope's field rotation, but the angle of the rotation changes slowly as the telescope moves. Overall, there are many reference stars observed during a satellite passage and they pass in random parts of the image, so the errors from the field rotation will also be random. Obviously, the average transform is not perfect, but is inevitable when short exposures are necessary. A camera with a relatively small CCD detector with very fast readout is preferred for LEO objects even at the expense of a small field of view, because otherwise the photometric sampling would be much worse. The emerging sCMOS technology might be able to solve that dilemma in the future.

Having usually only one star, a special two-step identification routine was developed. In the first step, frames that contain two or more reference objects are selected. Then the coordinates of the center of the image are calculated and compared with the telescope's coordinates obtained using the encoders. The differences between them reveal a systematic trend that is approximated with stiff spline and random deviations that are usually less than 3-5 arcsec. After subtracting the systematic trend from the telescope's coordinates we identify all other remaining objects. As the random errors of the telescope's coordinates are small, the identification is unambiguous. Nomad stellar catalog truncated to the 13th magnitude is used for object identification.

#### 5. DATA REDUCTION AND ASTROMETRY IN POZNAŃ

For the purpose of SST astrometry and photometry, a dedicated software suite has been developed in Astronomical Observatory of Adam Mickiewicz University. It consists of a number of tools specialized for a given task. The first tool is designed for detection of objects in an image. It calculates image background level map and performs an analysis of every pixel above the background level and user selected sigma level. In order to reduce noise when searching for objects, a 1-2 pixel symmetric image blur is used. The tool also performs initial selection, rejecting objects too close to edges, with too little or too many pixels or merging separate objects that are most likely different parts of a single trail. Finally, the

tool delivers a list of flux-weighted pixel coordinates for every object detected in an image. A total photometric signal and object shape parameter - elongation - is also calculated and saved for further analysis. The overall sensitivity limit of this tool is estimated at the level of S/N 2.

The second tool is used for identification of stars in an image with a stellar catalogue. Normally GAIA DR1 catalogue is used. The algorithm used for identification requires two input parameters: accurate image scale and estimated image RA and Dec. The efficiency of stellar field identification calculated as a ratio of identified frames to a total number of frames with sufficient number of stars is close to 99%. With PST1's field of view this corresponds to the fact that practically all frames are identified. With PST2 the percentage is lower because of limited number of reference stars. The absolute minimum number of reference stars required for identification is 3, but 4 or even 5 are usually used because overdetermination allows us to estimate errors at later steps.

The third tool is using Turner's method for calculating astrometric positions of all detected objects. It uses an iterative algorithm to reject the most deviating stars and automatically adjusts the order of astrometric solution to the number of stars available. The tool has been tested with regular long exposure time images and achieved standard deviation of measurement at the level of 20 mas for a sufficiently dense stellar field on PST2. In the case of satellite tracking images, which are usually taken using very short exposure times, the typical astrometric precision achievable is of the order of 0.5 arcsec because of differential seeing and other limitations.

The fourth tool is used to identify which object from the list of all observed objects is actually the target satellite. Since with different observing modes and exposure times it is possible to record long satellite trails as well as star-like images, object shape analysis has been rejected as a primary method of target identification. Instead, the algorithm is searching for an object (or several objects) that moves in a specific way. Initially the satellite tracking strategy is assumed and the search for nearly stationary objects on a set of images is performed. If this approach fails, then a sidereal tracking strategy is assumed and a search for linearly moving targets is performed. We found this approach quite successful in automatic identification of a satellite within a single series of images. Additionally, a search for deviating points using median line fitting (Theil-Sen estimator) is implemented to reject accidental detections of stars passing near the satellite image.

## 6. ORBITAL ANALYSIS IN ODESSA

Ajisai is a passive geodetic satellite with well known orbit. The International Laser Ranging Service (ILRS) publishes five days predictions for it. The NERC Space Geodesy Facility (SGF) provides one of these predictions

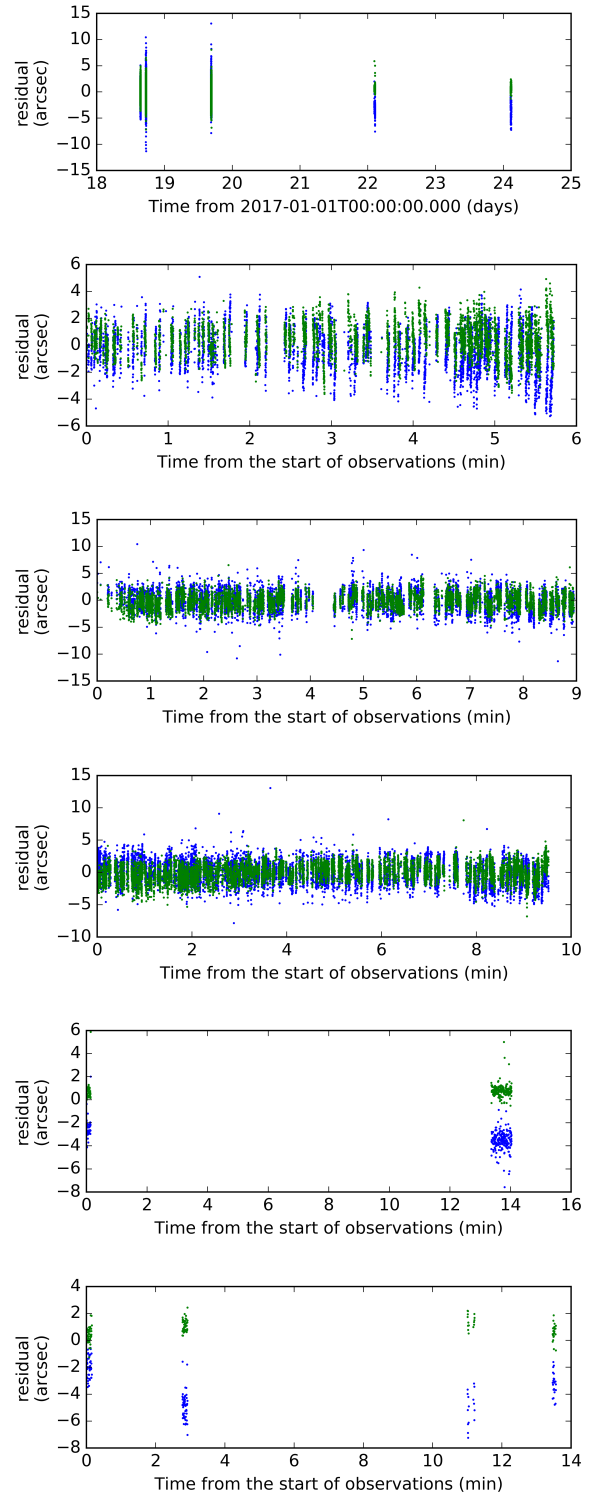


Figure 6. Residuals between Ajisai observations and SGF prediction. Blue points are residuals along the visible track; green points are residuals across the visible track. Top – the residuals for all tracks, other five – the residuals for each track separately. Odessa observations are presented in the second, third and fourth figure from top. Arizona observations are presented in two bottom figures.

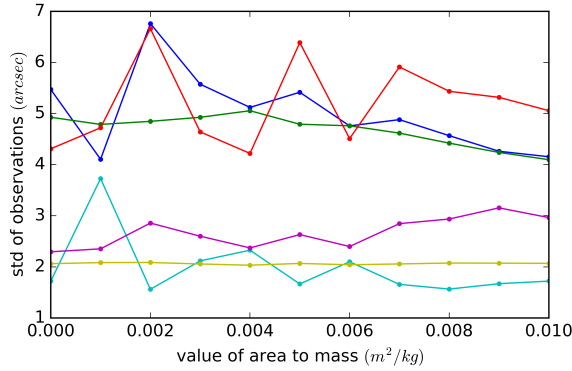


Figure 7. The estimation of standard deviations of observations with respect to fitted orbit for different values of assumed area to mass ratio. Light blue points correspond to the Arizona observations and the orbit fitting for 2 days interval; yellow points - the Odessa observations and the orbit fitting for 2 days interval; violet points - Odessa and Arizona observations and the orbit fitting for 2 days interval; red points - the Arizona observations and the orbit fitting for 7 days interval; green points - the Odessa observations and the orbit fitting for 7 days interval; blue points - the Odessa and Arizona observations and the orbit fitting for 7 days interval.

and it has reproducibility from one prediction to other. Five tracks of the satellite were obtained: three in Odessa and two in Arizona, covering the time span of 7 days. Therefore, 7 sequential SGF predictions were used for comparison with our observations. Predictions with the latest beginning date before the start time of the track were selected. Results of the comparison are shown in the Figure 6. We see that Odessa observations have significantly more random error than the observations obtained in Arizona. Simultaneously, the Arizona observations have a small systematic shift along tracks in relation to SGF prediction. This is to be expected based on different observing techniques used at both sites.

Topex/Poseidon and Jason-1 satellites were decommissioned and there are no accurate publicly available predictions for them. In this case numerical astrodynamics model implemented using low-level astrodynamics library Orekit<sup>2</sup> was used for the orbit estimation of these satellites. We chose the Cartesian coordinates for positions, velocities at orbit epoch and the area to mass ratio as the parameters of the numerical model of satellite motion. We use one parameter, the area to mass ratio, to calculate the influence of the atmosphere and the solar radiation pressure. The model of satellite motion takes into account the following forces:

1. the central gravitational attractor;
2. Eigen-6s truncated to the 51st degree and order for the gravitational attractions of the non-spherical Earth;

3. three-body gravitational attractions of the Sun and Moon (DE430);
4. FES2004 truncated to the 5th degree and order for gravitational attractions of oceanic tides;
5. gravitational attractions of solid-Earth tides of the Sun and Moon;
6. relativistic perturbation;
7. atmospheric drag forces for DTM2000 atmospheric model where solar activity was assumed as average;
8. solar radiation pressure including shadow function. We assume that the scattering of the solar radiation by the satellite is diffuse.

Numerical integrations were carried out using the Dormand-Prince method of 5(3) order with the step from 0.001 to 200 seconds. The integration tolerance (for the control of step size) is equal to 0.001 m for the integration of the motion equations in Cartesian coordinates. A dedicated code using Python language was developed in Odessa Observatory for determination of the model parameters using the least square method. The sum of squared residuals of observations and model equatorial coordinates (in the topocentric frame with axes parallel EME2000 on a sphere with radius 1) were minimized using Levenberg-Maquardt nonlinear fitting algorithm. In the process of estimating the model parameters we revealed that the best estimations of area to mass ratio of a satellite in the meaning of least square method depend on their prior values. Therefore, we had to calculate a grid of models for a sequence of these values (Figure 7).

In Figure 7 it is visible that the sum of square residuals for fitted orbits has many local minima. This makes it difficult to estimate the value of satellite's area to mass ratio. Moreover, the estimated standard deviation increases with the expansion of time span which was selected for fitting the orbit. For 2 days interval it is about 2 arcsec, for 7 days interval – about 5 arcsec. This reflects the fact that the orbital model used deviates from observations more for longer period of time. Considering the difficulties with the observational estimation of the area to mass ratio, only short time span (2-3 days) was fitted, where the atmospheric drag influence can be neglected and the area to mass ratio can be set to 0.0.

The residuals between observations obtained within interval of 2 days and the fitted orbits are presented in Figure 8. In all cases the observations obtained in Arizona occur in the first half of the day, the observations obtained in Odessa occur in the second half of the day. The Arizona observations have the value of random error of observations about 1.5 times less than the Odessa observations. In the case when both Odessa and Arizona observations were fitted together we see systematic differences between the model and observations. It is not clear whether the model of satellite motion is the cause of this or the observations have small systematic differences.

<sup>2</sup><https://www.orekit.org/>

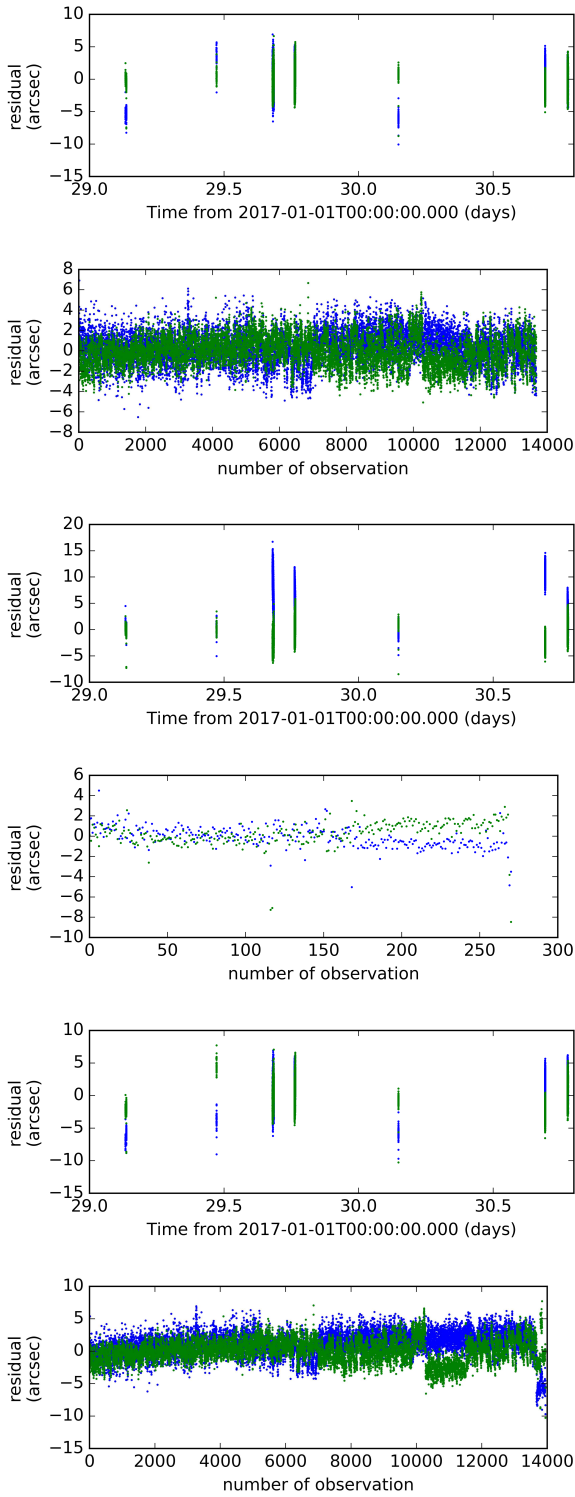


Figure 8. Residuals for Jason-1 satellite observations when only two days were fitted. Top two - only Odessa observations, middle two - only Arizona observations, bottom two Odessa and Arizona observations together. Blue points represent residuals along the visible track, green points - residuals across the visible track.

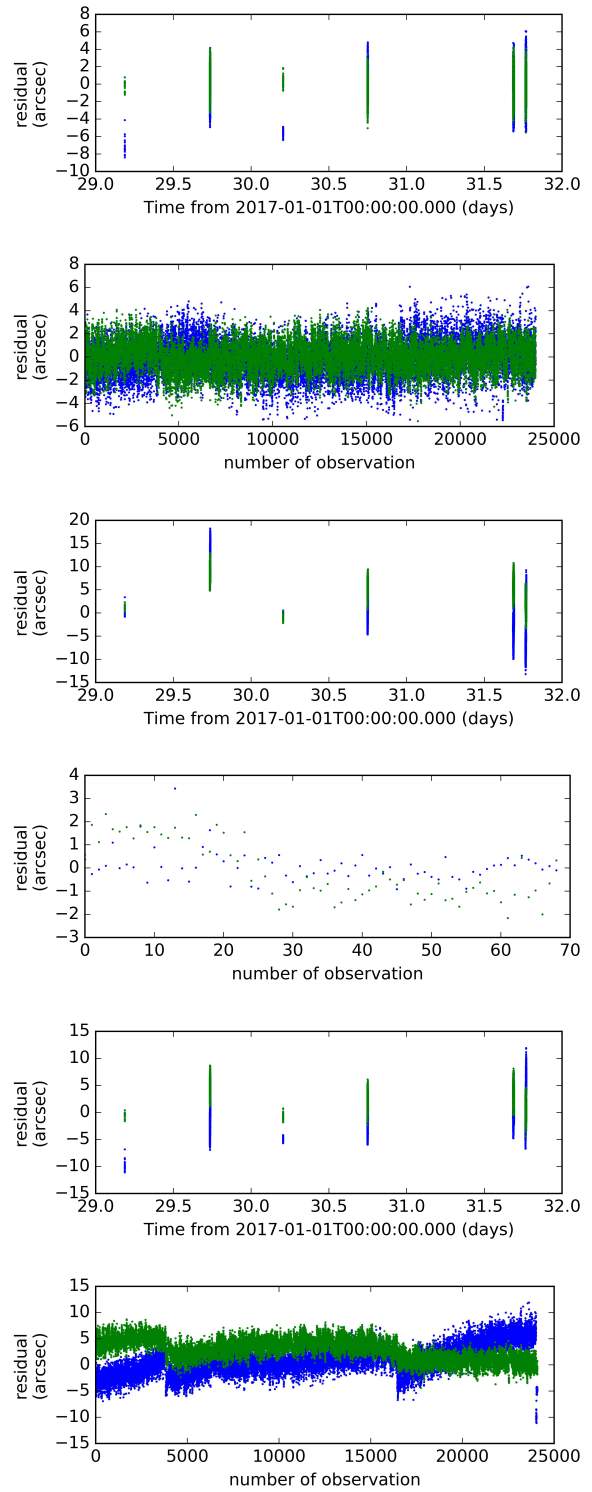


Figure 9. Residuals for Topex/Poseidon satellite observations. Top two - only Odessa observations, middle two - only Arizona observations, bottom two - Odessa and Arizona observations together. Blue points represent residuals along the visible track, green points - residuals across the visible track.

Table 1. Root mean square (RMS) values of the residuals along and across the satellite track.

	$RMS_{along}$ [arcsec]	$RMS_{across}$ [arcsec]	number of passes
<b>Jason-1</b>			
Arizona	1.05	1.29	3
Odessa	1.53	1.42	4
All	2.12	1.71	7
<b>Topex/Poseidon</b>			
Arizona	0.66	1.28	2
Odessa	1.45	1.22	4
All	2.84	3.47	6

Table 2. Dates of observations

	Arizona	Odessa
Jason-1	30–31.01.2017	30–31.01.2017
Topex	30–31.01.2017	30.01–1.02.2017

Similar analysis was carried out for Topex observations (Figure 9). Slightly larger estimated standard deviations for Topex observations than for Jason-1 (in the case when Odessa and Arizona observations were fitted together) are caused by longer time span of the orbit fitting. In this case systematic deviations of the model from the observations are clearly visible.

## 7. ORBITAL ANALYSIS IN POZNAŃ

Precise orbit determination of three satellites: Ajisai, Topex/Poseidon and Jason-1 has been performed with the use of the NASA/GSFC GEODYN II software [4] applied to astrometric observations in the form of right ascension and declination data.

The initial orbital elements of observed satellites have been taken from USSTRATCOM NORAD TLE Satellite Catalog. The mean elements from TLE were transformed to osculating elements with the use of an algorithm based on the Hori-Lie perturbation theory in the version of Mersman [5]. Next, the osculating elements were propagated to the moment of first observation with the use of Poznan Orbit Propagator STOP — software developed at the Astronomical Observatory of Adam Mickiewicz University [6]. The moment of the first observation is the epoch of the orbital initial elements. This moment is also the epoch of osculating elements obtained from GEODYN calculations with the use of given set of astrometric observations.

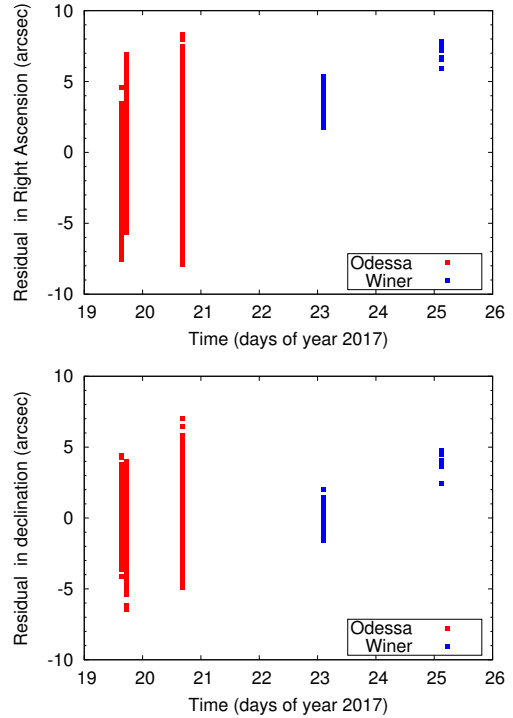


Figure 10. Residuals in Right ascension and declination [arcsec]. Object: Ajisai, Observatory: Odessa and Arizona.

The following force model has been taken into account:

- Earth gravity field: GRACE Gravity Model 03 (GGM03) up to 80 x 80 degree and order;
- Third body gravity: Moon, Sun and all planets with the use of DE403 JPL Ephemerides;
- Earth and ocean tides;
- Solar radiation pressure, including Earth's shadow effects;
- Atmospheric drag with NRLMSISE-00 model of the atmosphere.

The following values of the cross-sectional area to mass ratio ( $A/m$ ) parameter have been calculated on the basis of information about the size and mass of the satellites:

- Topex:  $A/m = 0.0035m^2/kg$ ;
- Ajisai:  $A/m = 0.0053m^2/kg$ ;
- Jason-1:  $A/m = 0.0066m^2/kg$ .

The orbit determinations of three satellites Ajisai, Topex/Poseidon and Jason-1 have been performed for three different cases, taking into account:

1. only observations from Arizona,

Table 3. Dates of observations.

	Arizona	Odessa
Topex	30 – 31.01.2017	30 – 31.01.2017
Jason-1	30 – 31.01.2017	30.01–2.02.2017
Ajisai	23 – 25.01.2017	19 – 20.01.2017

2. only observations from Odessa,
3. all observations from Arizona and Odessa.

The determined root mean square (RMS) values of the residuals in right ascension ( $\alpha$ ) and declination ( $\delta$ ) for Topex/Poseidon, Ajisai and Jason-1 are presented in Table 4.

The time span covered by the analysis is 4 days for Topex, 3 days for Jason-1 and 7 days for Ajisai. Table 3 contains dates of observations.

Example residuals for Ajisai calculated for the three abovementioned cases are presented in Figures 10 - 12. The RMS below 3 arcsec shows sufficient quality of observations both from Odessa and Arizona. The results meet the requirements set by the ESA and the EU SST Consortium for the accuracy of observations obtained by optical sensors. The orbit determinations performed when all observations are taken into account indicate small systematic differences between observations from Odessa and Arizona. These differences can be a result of different hardware and software solutions used by

Table 4. Root mean square (RMS) values of the residuals in right ascension ( $\alpha$ ) and declination ( $\delta$ ).

	$RMS_{\alpha}$ [arcsec]	$RMS_{\delta}$ [arcsec]	number of passes
<b>Topex</b>			
Arizona	0.85	0.51	2
Odessa	1.90	1.41	3
All	1.89	1.39	5
<b>Jason-1</b>			
Arizona	2.12	0.74	4
Odessa	3.29	1.15	3
All	3.74	1.24	7
<b>Ajisai</b>			
Arizona	1.29	1.8	2
Odessa	2.66	1.65	3
All	2.68	1.62	5

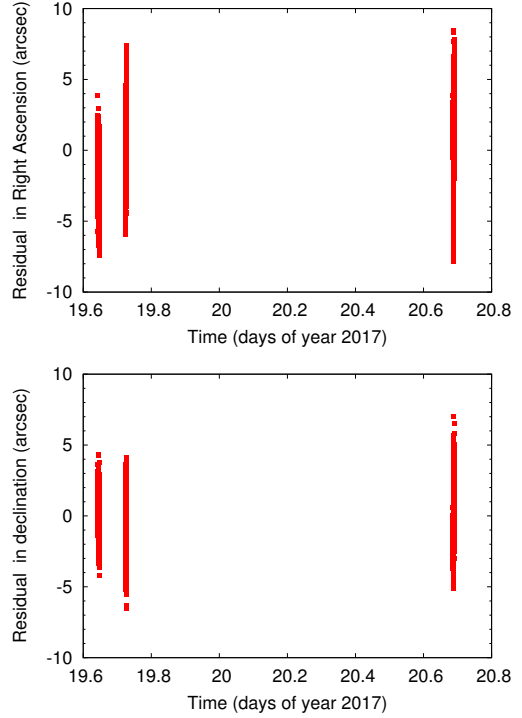


Figure 11. Residuals in right ascension and declination [arcsec]. Object: Ajisai, Observatory: Odessa.

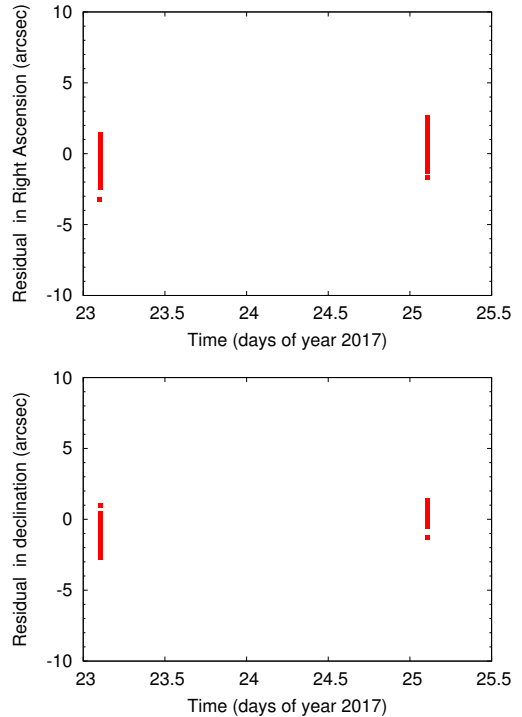


Figure 12. Object: Ajisai, Residuals in right ascension and declination [arcsec]. Object: Ajisai, Observatory: Arizona.

both groups: different observations and analysis procedures, different timing techniques and significantly different number of observations.

Eliminating these differences requires further cooperation to obtain comparable results with the use of the same standards by both Observatories.

## 8. PHOTOMETRY OF SATELLITES AND DETERMINATION OF ROTATION CHARACTERISTICS

An important problem that can be solved by observations of satellites and space debris is the determination of the characteristics of their rotation around the center of mass. For this purpose, brightness measurements of the target during its passage over the observation site is very useful, because large brightness variations can frequently be detected. Obviously, tracking a given target along its entire visible path is preferred in order to estimate its kinematic rotation parameters. From this point of view, observations from KT-50 sensor in Odessa are most suitable. Perhaps in the future, when the idea of a pre-flight comprehensive photometric description of a satellite is embodied, a small number of high-precision photometric measurements (in several optical ranges) will be sufficient to estimate the state of rotation by comparing them with the calculated values for the optical-geometric model of the satellite.

We present the results of determining the rotation characteristics of several space objects that have been observed during the joint 2017 campaign and data from long-term monitoring from Odessa.

Photometric lightcurves obtained for Topex/Poseidon satellite are presented in Figures 13 and 14. The period, which is revealed from the lightcurves from both observatories is close to 10.7 seconds. Figure 15 presents phased lightcurves. Brightness variations of Topex/Poseidon satellite have been systematically monitored for the last 7.5 years in Odessa. During this time, the rotation velocity of the ‘asymmetric’ satellite was constantly increasing, and the visible period decreased from 19 seconds to 10.7 seconds (Figure 16).

The rotation period of the inactive Envisat satellite has been monitored from Odessa between 2013 and 2015. In this case, the observed synodic period has increased from about 119 seconds to 161 seconds during over 3 years. With such a long period it is important to correct the observed period for the effect of change of satellite’s phase angle during its observation. Assuming the rotation axis is tilted at the angle of  $60^\circ$  to its orbit, we calculated the values of the sidereal (inertial) rotation period for the prograde and retrograde case (Figure 17 top). Assuming the rotation axis is perpendicular to the orbital plane, we see a noticeable decrease in the scatter of the estimates of the inertial period obtained for the retrograde sense of rotation (Figure 17 bottom).

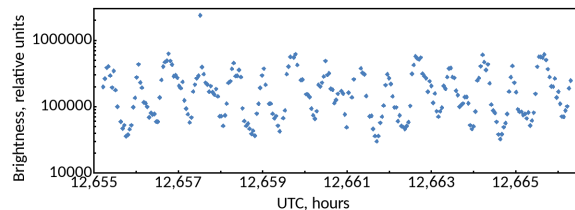


Figure 13. The lightcurve of the inactive Topex/Poseidon satellite (ceased operation in October 2006), obtained with PST2 70 cm telescope in Arizona on January 25, 2017.

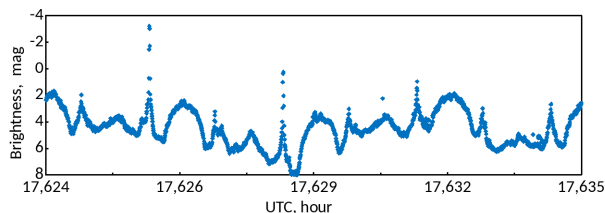


Figure 14. A fragment of the lightcurve of the Topex/Poseidon satellite obtained on January 30, 2017 in Odessa on a KT-50 telescope.

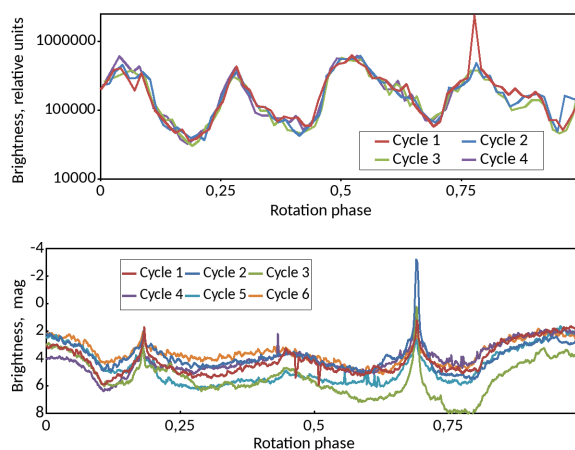


Figure 15. The phase convolution of the Topex/Poseidon light curves, which are shown in Figures 13 and 14.

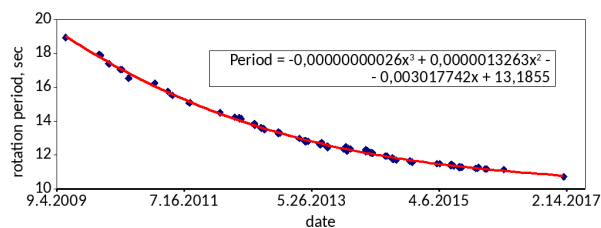


Figure 16. The change in the visible period of Topex/Poseidon rotation during 7.5 years.

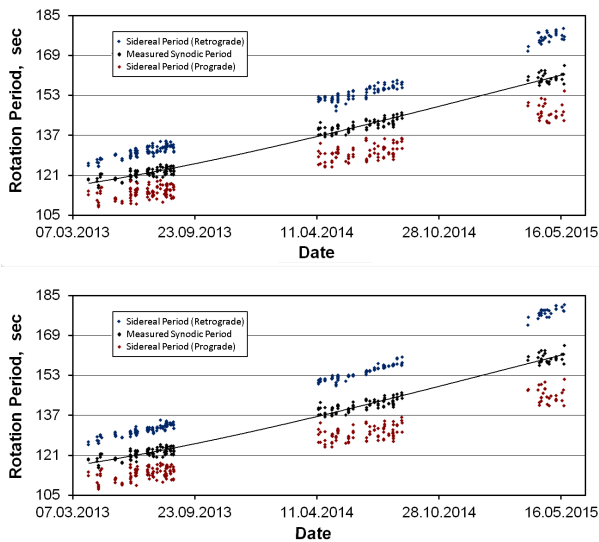


Figure 17. Rotation period of Envisat observed from Odessa Observatory (black dots). Red and blue dots indicate the corresponding values of the sidereal (inertial) rotation period of the satellite for the prograde and retrograde sense of rotation about the rotation axis. At top panel we assumed that the rotation axis inclination with respect to its orbital plane is 60 degrees, at the bottom panel results for perpendicular rotation axis are presented. A noticeable decrease in the scatter is visible for the inertial period obtained for retrograde rotation around perpendicular axis.

Table 5 shows the RMS values of the sidereal periods scattering with respect to the polynomial fit, for two positions of the rotation axis and two senses of the Envisat rotation.

This method of estimation of rotation parameters was also used for another inoperative Cbers-2b satellite [7].

Figure 18 shows a photograph of the Japanese experimental geodetic satellite (EGS) Ajisai (1986-61A). This satellite is not a space debris, but it is a passive object and its movement around the centre of mass is a good indicator of the effect of cosmic conditions (different forces and torques) on the rotation of the satellite. The Ajisai satellite has 318 small fragments of the spherical mirror with a radius of 9 m on the surface and its light curve demonstrates a dense series of light flashes during the passage (Figure 19).

Figure 18 shows the conditional model of the mirrors arrangement on the Ajisai surface, as a result of multiple observations and timing of the moments of the light flashes of the satellite calculated in Odessa. One color shows mirrors located in one belt, but having different slopes relative to the mid-latitude of the belt. Empty squares represent the location of the blocks of laser reflectors.

Figure 20 shows the phase convolution of the abovementioned

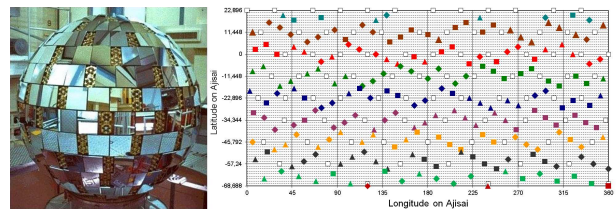


Figure 18. The Ajisai satellite (photo left) and the model of arrangement of mirrors on the Ajisai surface (right).

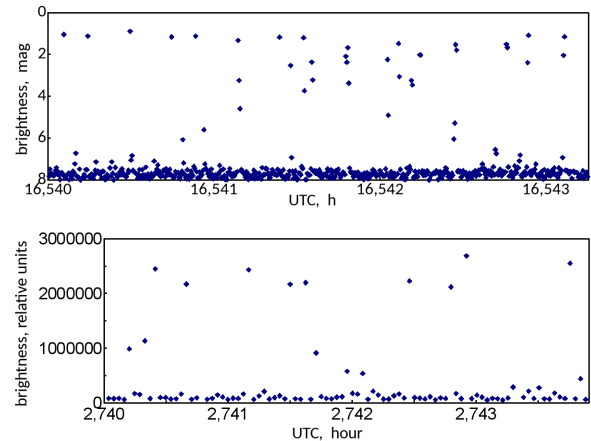


Figure 19. Two fragments of Ajisai lightcurves: received in Odessa on January 20, 2017 (top); and received in Arizona on 25 January 2017 (bottom).

tioned Ajisai lightcurve obtained in Odessa, with a rotation period of 2.344 seconds, and the corresponding fragment of the Ajisai model representing the location of the mirrors responsible for the observed light flashes. We note that the phases of the light flashes correspond well to the longitude position of six mirrors on two adjacent subbelts, which in the considered part of the lightcurve participate in the reflection of sunlight due to partially overlapping indicatrices.

Figure 21 shows the phase convolution of the abovementioned Ajisai lightcurve obtained in Arizona, with a period of 2.345 seconds, and corresponding fragment of the Ajisai model, representing the location of the mirrors responsible for the observed light flashes.

We see a very good agreement between two independent measurements of the rotation period of Ajisai. In addition, we see that the Ajisai brightness measurements made in Arizona well correspond to the prediction of the flashes moments, made on the basis of the satellite's model constructed from the measurements taken in Odessa.

As a result of photometric monitoring of Ajisai during 2009-2017, as well as the use of the model, all the basic parameters of the passive satellite rotation - the period and sense of rotation, the secular variation of the rotation speed (deceleration), the rotation speed varia-

Table 5. The standard deviations of sidereal periods for two positions of the pole and sense of Envisat rotation.

Spin axis orientation	Spin axis is perpendicular to the orbital plane ( $u = 0^\circ$ )		Spin axis makes the $60^\circ$ angle with the orbital plane ( $u = 30^\circ$ )	
	Retrograde rotation	Prograde rotation	Retrograde rotation	Prograde rotation
2013	0.960	2.184	1.380	2.205
2014	1.047	2.643	1.822	2.716
2015	1.214	3.139	1.935	3.661
2013-2015	1.029	2.504	1.642	2.649

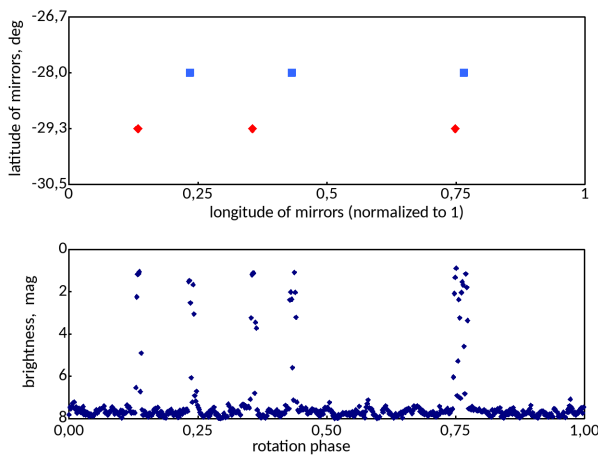


Figure 20. Fragment of the model of the mirrors arrangement on Ajisai responsible for the observed light flashes (top) and phase convolution with period of 2.344 seconds, given above the Ajisai lightcurve obtained in Odessa (bottom).

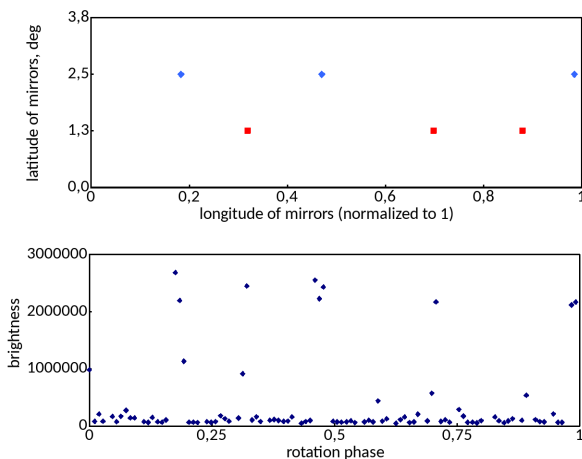


Figure 21. Fragment of the model of the mirrors arrangement on Ajisai responsible for the observed light flashes (top) and phase convolution with period of 2.345 seconds, given above the Ajisai lightcurve obtained in Arizona (bottom).

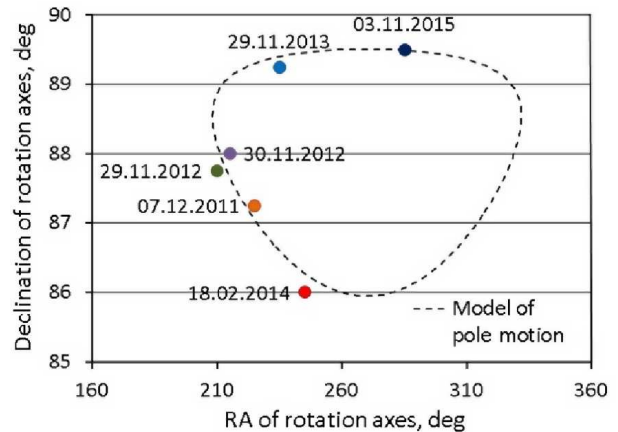


Figure 22. The trajectory of nutation oscillations of the Ajisai rotation pole with a period of 117.1 days.

tions (caused by the solar radiation pressure), estimation of the period of nutation oscillations and the precession displacement of the Ajisai rotation axis were obtained. Figure 22 shows the trajectory of nutation oscillations of the Ajisai rotation pole with a period of 117.1 days, obtained from the results of the photometry of the satellite in Odessa (N. Koshkin et al. / Ajisai spin-axis precession and rotation-period variations from photometric observations // in press).

Permanent photometric monitoring by the “Ukrainian network of optical stations” (UMOS) of several hundred different satellites and space debris on low orbits is reflected in the periodic edition of the “Atlas of light curves of space objects”<sup>3</sup> and will be presented in full on the ftp server of the National Space Center of Ukraine<sup>4</sup>.

## 9. CONCLUSIONS

A joint Polish-Ukrainian campaign using two different telescopes, astrometric techniques, timing systems and orbital analysis tools have been successfully carried out.

<sup>3</sup><http://dSPACE.onu.edu.ua:8080/handle/123456789/8480>

<sup>4</sup><http://195.16.76.195:3000/satellites>

The overall random errors in astrometry are slightly higher (about 1.5 times) in Odessa than in Arizona. This is understandable, because all satellite positions from Arizona were derived using astrometric solution utilizing minimum 5 reference stars, whereas Odessa is usually using a one-star solution. On the other hand, the sensor in Odessa is able to track LEO satellites much longer and with a higher frame rate, resulting in better statistics and better photometric and astrometric coverage.

Both orbital fitting techniques, using GEODYN II in Poznań and OREKIT in Odessa show similar results. When analysing data from a single sensor, the data points fit considerably better, with less pronounced systematic deviations. When analysing data from both sensors together, the systematic errors are better visible at the level of a few arcsec. This might be a result of a small time bias at one or both sites, at the level of 0.01 sec or smaller. Even so, both sensors are already capable of providing astrometric measurements of LEO targets meeting ESA SST and EU SST requirements for accuracy.

The photometric analysis of satellites with short rotation periods - Ajisai and Topex/Poseidon - revealed clear periodic brightness variations in the data from both sensors. Individual specular reflections from Ajisai mirrors are distinguishable because of relatively high framerate on both sensors (6 and 25 fps). It was possible to identify individual mirrors using the satellite's shape model. Long-term monitoring from Odessa revealed period changes of Envisat and Topex/Poseidon. A method of rotation axis orientation based on the analysis of scatter of period determinations has been presented and applied for Envisat data proving its retrograde rotation and spin axis perpendicular to its orbital plane.

## REFERENCES

1. Putney, B., Kolenkiewicz, R., Smith, D., Dunn, P., Torrence, M.H. (1990), Precision orbit determination at the NASA Goddard Space Flight Center, *Advances in Space Research*, Vol. **10**, No. 3–4, pp. 197-203.
2. Kouprianov, V. (2008), Distinguishing features of CCD astrometry of faint GEO objects, *Advances in Space Research*, **41**(7), 1029–1038.
3. Shakun, L. S., Koshkin, N. I. (2013), Determination of visible coordinates of the low-orbit space objects and their photometry by the CCD camera with the analogue output. Initial image processing. *Advances in Space Research*, **12**, 2010
4. Pavlis, D. E., Rowlands, D. D., et al. (1998), GEODYN Systems Description, vol.3. NASA Goddard, Greenbelt.
5. Wnuk, E., (1999). Relation Between Osculating and Mean Orbital Elements in the Case of the Second Order Theory, *AAS paper 99-448*, *Advances in the Astronautical Sciences*, **103**, 2279-2292.
6. Wnuk, E. (2015), STOP - The Short-Term Orbit Propagator, KePassa2015, 28-30 October 2015 Toulouse.
7. Koshkin, N., Korobeynikova, E., Shakun, L., Strakhova, S., Tang, Z.H. (2016) Remote Sensing of the Envisat and Cbers-2B satellites rotation around the centre of mass by photometry, *Advances in Space Research*, **58**(3), 358-371.